Xe nanocrystals in Si studied by x-ray absorption fine structure spectroscopy

Giuseppe Faraci* and Agata R. Pennisi
Dipartimento di Fisica e Astronomia, MATIS—Istituto Nazionale di Fisica della Materia, Universitá di Catania, Via Santa Sofia 64, 95123 Catania, Italy

Federico Zontone
European Synchrotron Research Facility (ESRF), BP 220, F-38043 Grenoble Cedex, France
(Received 31 January 2007; revised manuscript received 17 April 2007; published 19 July 2007)

The structural configuration of Xe clusters, obtained by ion implantation in a Si matrix, has been investigated as a function of the temperature by x-ray absorption fine structure spectroscopy. In contrast with previous results, we demonstrate that an accurate analysis of the data, using high order cumulants, gives evidence of Xe fcc nanocrystals at low temperature, even in the as-implanted Si; expansion of the Xe lattice is always found as a function of the temperature, with no appreciable overpressure. We point out that a dramatic modification of these conclusions can be induced by an incorrect analysis using standard symmetrical pair distribution function $G(r)$; for this reason, all the results were checked by x-ray diffraction measurements.

DOI: 10.1103/PhysRevB.76.035423 PACS number(s): 36.40.Ei, 61.10.Ht, 61.43.−j, 61.46.Hk

I. INTRODUCTION

In the last two decades, the confinement of rare gas clusters into a solid matrix was often achieved by ion implantation. These clusters were observed in a pressurized solid or fluid phase[1–15] by several techniques including x-ray absorption spectroscopy[3–5] and x-ray diffraction (XRD).[9,14]

In a metal matrix at temperatures lower than the solid gas melting point, crystalline rare gas nanoaggregates are detected with contracted interatomic distances as a consequence of the surface pressure exerted by the host lattice.[14] In semiconductors, mainly for Kr and Xe agglomerates implanted in a Si matrix, many contrasting results have been recently published.

Actually, x-ray absorption fine structure (XAFS) investigation of as-implanted Kr in Si did not show any evident XAFS structure,[5] although clear evidence of clustering was obtained. In a Si matrix, precipitates of Xe were clearly detected in the crystal phase only after annealing.[3,12] This result was explained via the strong influence due to the semiconductor recrystallization during the annealing. In fact, the implantation process at ambient temperature does amorphize a semiconductor. Therefore, for Xe implanted in Si, around and beyond the melting point, there is discrepancy between the earlier interpretation of XAFS data[3] and recent XRD investigations.[9] Actually, at room temperature, the XAFS measurements showed a very low coordination, whereas XRD data found evidence of a fluid phase with coordination six times larger.

For the aforementioned reasons, we revisited the Xe clustering in Si, collecting, for several samples, high flux XAFS spectra as a function of the temperature, in the range of 10–300 K. The technique allows the geometrical characterization of an ensemble of clusters giving the average first, second, and third coordination shell distance, coordination number, and relative vibrational amplitude.[16,17] The same samples were also checked by XRD as a function of the temperature, monitoring the Xe diffraction peaks.[18] These last data gave information about the phase, the lattice parameter, and the size of the Xe agglomerates, permitting a crossed verification of the XAFS parameters and guiding the correct determination of high order cumulants.

The excellent quality of the data allows us to clarify all the previous controversial points, by comparing XAFS analyses and XRD results. We show evidence of Xe nanoclusters in as-implanted as well as in annealed Si with different average sizes in the two cases. We emphasize that, whereas standard analysis of the XAFS data gives (as claimed in the past) a pressurized lattice parameter for solid Xe agglomerates, in annealed samples, the use of higher order cumulants permits the extraction of *normal* features for Xe nanocrystals embedded in Si substrates. Only in as-implanted samples we get a somewhat reduced lattice parameter for Xe nanocrystals randomly oriented into the Si matrix.

The XRD data, reported in detail in Ref. 18, confirm that a correct XAFS analysis should use for rare gas nanocrystals high order cumulant correction. In fact, we obtain (i) fcc Xe nanocrystals, at temperature lower than the transition point, with different average sizes in as-implanted and in annealed samples, (ii) size dependent lattice parameters according to the preparation conditions, and (iii) lattice expansion as a function of the temperature.

II. EXPERIMENT

The experiment was performed at the BM32 beamline of the European Synchrotron Radiation Facility (ESRF), Grenoble, France; experimental details can be found in Ref. 5. X-ray spectra were collected in the range of 4650–5100 eV by detection of the Xe L_3 fluorescence yield. The energy resolution was better than 10^{-4}. In order to improve the statistical collection of the data, the fluorescence radiation was collected by a 30-element ultrapure Ge detectors cooled at 77 K. A He cryostat was used to maintain the sample temperature at 10, 50, 150, 200, and 300 K within ±1 K. The sample was at 45° with respect to the beam and to the fluorescence detector. We observed two kind of samples: as implanted and annealed after implantation. The implantation energy was 100–200 keV. The implantation temperature was 300 K. The substrate was a Si(100) single crystal

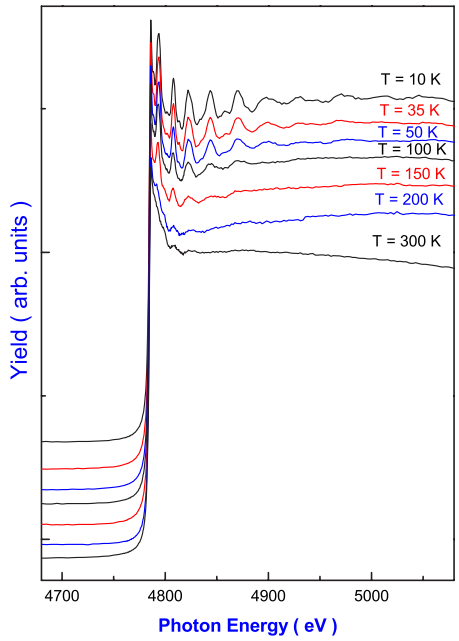

FIG. 1. (Color online) Fluorescence yield spectra as a function of the energy, for several temperatures. The threshold and the XAFS oscillations are well visible at low temperature. The spectra are vertically shifted for clarity.

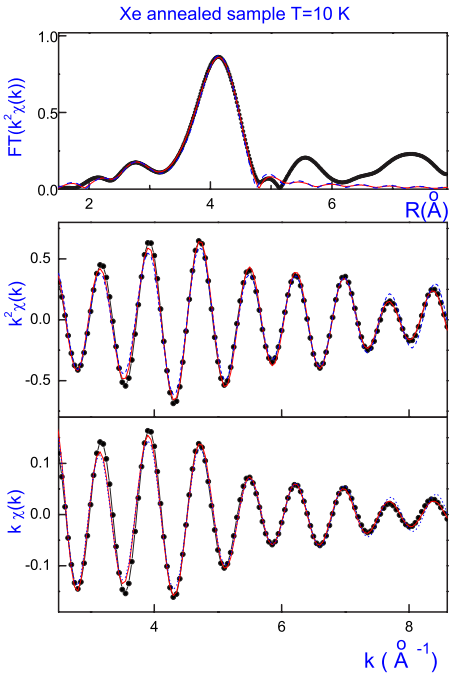

FIG. 2. (Color online) Upper graph: Fourier transform (dotted line) of the XAFS spectrum $\chi(k)$ weighted by k^2, for the annealed spectrum at $T=10$ K. Middle graph: XAFS oscillations (dotted line) weighted by k^2 as a function of the wave vector, for the annealed spectrum at $T=10$ K. Lower graph: XAFS oscillations (dotted line) weighted by k as a function of the wave vector, for the annealed spectrum at $T=10$ K. In all the graphs, the fits obtained for the Si-Xe and Xe-Xe first shells, using the FEFF code, are also reported with (continuous line) and without (dashed line) cumulant corrections. The agreement between experimental data and best fit is quite good in both cases.

wafer, 0.5 mm thick. As reported elsewhere,[3,9] the implantation profile is a Gaussian curve centered about 100 nm under the Si surface. The annealing temperature was therefore limited to 700 °C in order to limit Xe outgassing. All the samples were implanted at the maximum fluence (10^{17} at./cm^2), always at room temperature. As the Xe layer was sufficiently thin in a light matrix, no correction was applied for self-absorption. The normalized fluorescence spectra I_f/I_0 were analyzed according to a standard procedure, removing the background by means of a cubic spline. The spectrum was analyzed in the k range of 2.3–8.5 Å^{-1}, limited by the growth of the L_2 absorption peak. Actually, the IFEFFIT package[16,17,19] was used for the extraction of the signal from the raw data.

III. RESULTS AND DISCUSSION

In Fig. 1, we display typical raw absorption spectra with evident XAFS oscillations for some values of the temperature in an annealed sample. As clearly seen in the figure, the amplitude of the features is well pronounced at 10 K, somewhat decreasing as the temperature increases, with a very strong attenuation at $T=150$ K. In Fig. 2, the $\chi(k)$ oscillations weighted by k and k^2 are displayed with the Fourier transform (FT) of the $k^2\chi(k)$ for the annealed sample at the lowest temperature. In this case, as proved in the following, the peaks correspond to the Si-Xe interface distance and Xe-Xe first, second, and third shells, respectively, since at 10 K Xe condenses, with a fcc lattice, within the Si cavities formed by the implantation process. A quantitative analysis can be performed by a fitting procedure on the XAFS oscillations and/or on the FT curve. We adopted a very accurate method, named FEFF,[19,20] including curved wave effects, multiple scattering paths, and inelastic losses. The fit can provide the best values for the unknown parameters, namely, the coordination number N, the distance R, and the Debye-Waller (DW) factor σ^2 for each shell. We also point out that at the lowest temperature, the XAFS (S_0^2) amplitude factor[21] was obtained equal to 1.0, with high reliability, and therefore fixed at this value elsewhere. In the fitting procedure, the E_0 value was in addition always obtained with good accuracy in the range of 0.7 ± 0.1 eV.

All the analyses were done taking great care to avoid any overestimation[22,23] of the correlated parameters N and σ^2 and fitting both the first shell XAFS oscillations and the Fourier transforms, as reported in Fig. 2, where a comparison of the $k\chi(k)$ and $k^2\chi(k)$ with the corresponding fits is displayed. This analysis without higher order correction was extended to the data taken for the entire set of temperatures, for both samples (with and without annealing). The extracted fitting parameters are reported in Table I. The accuracy of the fits was evaluated, as usual, comparing the χ^2 (or the R factor).[24] The best fit values, as seen in Fig. 2, are in good agreement with the experimental data. However, in order to take into account the asymmetrical pair distribution function $G(r)$ of van der Waals Xe bonds, we introduced in the analysis higher order cumulants,[25,26] which correct for non-Gaussian $G(r)$ distributions. This is a crucial point in the present

TABLE I. Fit parameters of the first shell Xe-Xe around a Xe absorber obtained by the FEFFIT code for the annealed sample. The average size of the Xe nanocrystals is evaluated at 340 Å. The uncertainty for the coordination number is of the order of ±0.2, for the distances ±0.01, and for the DW factors and for the cumulants ±5.0%. Note the dramatic difference in the fitted distances when no cumulants σ_3 and σ_4 are used. The last column reports the Xe-Xe value deduced from XRD data with accuracy better than 0.002 Å.

T (K)	N	R (Å)	σ^2 (10^{-4} Å^2)	σ_3 (10^{-4} Å^3)	σ_4 (10^{-4} Å^4)	R (Å) (XRD)
10.	11.3	4.36	107.			4.348
35.	11.6	4.34	162.			4.349
50.	10.9	4.32	214.			4.350
100.	8.5	4.29	353.			4.389
150.	4.9	4.24	357.			4.448
10.	11.3	4.34	61.	−5.	−3.	4.348
35.	10.6	4.35	90.	0.3	−4.	4.349
50.	9.4	4.36	120.	12.	−6.	4.350
100.	6.9	4.38	120.	51.	−25.	4.389
150.	4.5	4.44	137.	100.	−32.	4.448

analysis because apparently good fits can be obtained without any cumulant, as done in the previous work.[3] In Fig. 2, also the fits with cumulant corrections are shown for the XAFS oscillations. Here, the agreement with the experiment is excellent. It is clear that the overall fits are very similar, although, as expected, the χ^2 improves in the presence of high order corrections. In this case, however, the obtained parameters change dramatically. As shown in Table I, the use of cumulants gives Xe lattice expansion as a function of the temperature and not the contraction deduced if no cumulant correction is introduced. Of course, there is no *a priori* justification for using a given number of cumulants. Therefore, only an accurate comparison between the various hypotheses within guided XAFS analyses can give the correct solutions and the best fit values. A cross-check with other techniques is therefore extremely valuable.

In order to ascertain whether the use of the cumulants was appropriate and for verifying the reliability of the fitted parameters, we investigated, as already mentioned, the *same* samples as a function of the temperature by XRD. As detailed elsewhere,[18] the diffraction data confirm the presence of Xe fcc nanocrystals, providing the Xe lattice parameters at each temperature. Of course, this information was used to guide the XAFS analyses, obtaining the definitive confirmation of the validity of the cumulant correction.

In Fig. 2, the fit obtained on the Fourier transform of $k^2\chi(k)$ using the fcc parameters of a Xe cluster, having Si at its boundaries, is included. In this case for the annealed sample, around a Xe central atom we obtain, at 10 K, 11 Xe atoms in first shell at a distance of 4.34 Å, 5 Xe atoms in second shell at a distance of 6.05 Å, and 24 Xe atoms in the third shell at a distance of 7.56 Å. One additional silicon atom is also present in first shell at 3.37 Å from the Xe central atom denoting an ordered Si-Xe interface, as confirmed by the XRD and transmission electron microscopy data analysis.[18] The reported parameters do not include any multiscattering contribution because of its negligible influence on the second shell; the third shell could be fitted only at the lowest temperatures, and therefore its parameters were not refined at all.

The previous results denote an ensemble of large crystalline clusters which have sizes large enough to give an average Xe-Xe first coordination differing by only 1 from the fcc crystal value; the single Si atom found in the first shell is clearly due to an epitaxial condensation of Xe on the silicon walls at the cluster interface with the matrix. This is confirmed by XRD, which reveals a Xe epitaxial alignment with the Si matrix for the annealed sample. We present now the global results obtained for the annealed and for the as-implanted samples as a function of the temperature. In Tables I and II, these results are resumed for the first shell. We distinguish between the as-implanted and the annealed samples. First of all, we find clear evidence of the presence of Xe nanocrystals also in the as-implanted Si. Comparing the coordination numbers at $T=10$ K, we observe, however, a strong difference caused by the annealing. In fact, in the as-implanted Si, the reduced value of the coordination of the first shell indicates a higher contribution of surface Xe, i.e., smaller clusters. In the as-prepared sample, a second reason for the coordination lowering can be attributed to an incomplete filling of the shells of the fcc crystal containing therefore some voids and/or some silicon atoms trapped in substitutional position in the Xe lattice. Note also that a more disordered Xe-Si interface is evidenced by a very low Xe-Si coordination.

On the other hand, in the annealed sample the thermal process has favored a more compact aggregation of the fcc structure with a complete filling of the various shells. Therefore, a possible scenario can be constituted by the presence of crystalline bubbles whose sizes are larger when the annealing procedure induces the agglomeration of smaller bubbles. This explains why the cluster ensemble for an annealed sample gives a first and a second coordination close to those of the fcc Xe crystal. It should be stressed that the reported values are averaged over the cluster distribution, taking also into account the presence of a large number of single Xe atoms or very small clusters diffused in the matrix, with a significant decrease of the coordination numbers even at low temperature. This is an important difference with re-

TABLE II. Fit parameters of the first shell Xe-Xe around a Xe absorber obtained by the FEFFIT code for an as-implanted sample. The average size of the Xe nanocrystals is evaluated at 45 Å. The uncertainty for the coordination number is of the order of ±0.2, for the distances ±0.01, and for the DW factors and for the cumulants ±5.0%. Note the dramatic difference in the fitted distances when no cumulants σ_3 and σ_4 are used. The last column reports the Xe-Xe value deduced from XRD data with accuracy better than 0.002 Å.

T (K)	N	R (Å)	σ^2 (10^{-4} Å^2)	σ_3 (10^{-4} Å^3)	σ_4 (10^{-4} Å^4)	R (Å) (XRD)
10.	7.5	4.33	120.			4.317
50.	6.5	4.29	220.			4.348
100.	3.7	4.22	320.			4.391
150.	1.8	4.15	400.			4.433
10.	5.6	4.31	10.	−8.	−12.	4.317
50.	4.7	4.35	10.	30.	−24.	4.348
100.	2.9	4.38	40.	85.	−20.	4.391
150.	1.5	4.44	30.	86.	−20.	4.433

spect to the diffraction technique detecting only coherent contributions. Furthermore, an incomplete filling of the condensed Xe bubbles implies many vacancies and therefore lower coordination numbers and higher DW factors, when the absence of interatomic forces allows wider vibrational amplitudes; a similar effect should be expected for the presence of stacking faults, dislocations, and similar defects. These can cause the fragmentation of large clusters when the temperature increase can favor the separation of large clusters in many smaller agglomerates. An additional information can be gained by the comparison of the Si-Xe shell well evident in the annealed sample, but not at all in the as-implanted one. It is a clear evidence of an epitaxial condensation of the Xe clusters on the Si matrix when the sample is annealed; otherwise, the clusters are randomly oriented in an amorphous matrix and no Si-Xe shell can be seen.

It is worth noting that at all temperatures (see Tables I and II) if no cumulants are used, the nearest-neighbor distance is slightly reduced with respect to the crystal value. This contraction in the past was attributed to the pressure exerted by the host lattice;[9,12] the wrong conclusion of an overpressure increasing with the temperature is now disproved by the correct cross analysis using XAFS and XRD.

Lattice expansion as a function of the temperature is instead obtained by the model using the cumulants' contribution. A slight overpressure at $T=10$ K is still evident, however, in the as-implanted sample because of the very small size of the clusters. Here, the pressure $P=2\gamma/r$ is reflected by the reduced DW factors and by the slightly (1%) contracted Xe nearest-neighbor distance, with respect to larger as-implanted samples.[18]

The present results provide the solution of the intriguing contrasts arising in the literature. A correct analysis of the XAFS data both for the as-implanted and for the annealed samples demonstrated the expansion of the Xe nanocrystals for increasing temperature (see Tables I and II). Therefore, XAFS and XRD results are now mutually consistent for both samples, i.e., for average Xe cluster sizes of about 300 and 45 Å. The first coordination number's difference in the two samples is now explained because of the different surface-to-volume contributions, implying an average value more and more reduced as the cluster size decreases. We emphasize that Xe nanocrystal expansion as a function of the temperature, without any overpressure, modifies the previous description given in the literature. Xe behaves in Si as an ensemble of normal rare gas bubbles condensing in cavities large enough to allow expansion without any overpressure due to the host lattice. However, the first coordination number for the annealed sample was found very close to the bulk value, denoting large clusters and a reduced number of single Xe atoms diffused in the matrix. As the temperature increases, the first coordination number is progressively reduced very likely because of cluster fragmentation along stacking faults or dislocations. Similar behavior is observed for the as-implanted sample. At 150 K, the transition temperature is approached. The XAFS signal is very much reduced. A solid-to-fluid transition is observed. As the XRD data confirm with high precision,[18] the transition temperature is size dependent. At 200 and 300 K, the XAFS data show a complete absence of an ordered phase and we conclude that a fluid disordered Xe phase is now filling the Si cavities. In the present case, no solid or amorphous Xe cluster survives in contrast with Kr behavior in a metal.[14]

A final comment is deserved by the high values of the Debye-Waller factors and of the cumulants, denoting a behavior typical of van der Waals forces weakly interacting through the Lennard-Jones potential. The values of the cumulants could be attributed not only to the asymmetrical $G(r)$ distribution but also to a possible distorted charge vibration along specific crystalline orientations. The presence of stacking faults, evident in the XRD data concerning the Xe(111) peak, certainly should influence this behavior.

ACKNOWLEDGMENTS

We are grateful to the ESRF staff and to Olivier Proux of the BM32 beamline for the excellent collaboration during the measurements. Thanks are due to M. Parolin and D. Boscarino for providing some of the samples and to F. D'Acapito for helpful discussions. We thank also Andrew Fitch for a critical reading of this paper.

*giuseppe.faraci@ct.infn.it

[1] A. vom Felde, J. Fink, Th. Müller-Heinzerling, J. Pflüger, B. Scheerer, G. Linker, and D. Kaletta, Phys. Rev. Lett. **53**, 922 (1984).
[2] E. Fleischer and M. G. Norton, Heterog. Chem. Rev. **3**, 171 (1996).
[3] G. Faraci, A. R. Pennisi, A. Terrasi, and S. Mobilio, Phys. Rev. B **38**, 13468 (1988); G. Faraci, in *Fundamental Aspects of Inert Gases in Solids*, NATO Advanced Studies Institute, Series B: Physics, edited by S. E. Donnelly and J. H. Evans (Plenum, New York, 1991), Vol. 279, p. 251.
[4] G. Faraci, S. La Rosa, A. R. Pennisi, S. Mobilio, and G. Tourillon, Phys. Rev. B **43**, 9962 (1991).
[5] G. Faraci, A. R. Pennisi, and J. L. Hazemann, Phys. Rev. B **56**, 12553 (1997).
[6] A. Polian, J. P. Itie, E. Dartyge, A. Fontaine, and G. Tourillon, Phys. Rev. B **39**, 3369 (1989).
[7] C. J. Rossouw and S. E. Donnelly, Phys. Rev. Lett. **55**, 2960 (1985).
[8] R. C. Birtcher and W. Jaeger, J. Nucl. Mater. **135**, 274 (1985); R. C. Birtcher, *Fundamental Aspects of Inert Gases in Solids* (Ref. 3), p. 133.
[9] F. Zontone, F. D'Acapito, G. Faraci, and A. R. Pennisi, Eur. Phys. J. B **19**, 501 (2001).
[10] M. Wittmer, J. Roth, and J. W. Mayer, J. Appl. Phys. **49**, 5207 (1978).
[11] A. Luukkainen, J. Keinonen, and M. Erola, Phys. Rev. B **32**, 4814 (1985).
[12] C. Templier, B. Boubeker, H. Garem, E. L. Mathe', and J. C. Desoyer, Phys. Status Solidi A **92**, 511 (1985).
[13] C. Templier, H. Garem, and J. P. Riviere, Philos. Mag. A **53**, 667 (1986).
[14] H. H. Andersen, J. Bohr, A. Johansen, E. Johnson, L. Sarholt-Kristensen, and V. Surganov, Phys. Rev. Lett. **59**, 1589 (1987).
[15] P. Revesz, M. Wittmer, J. Roth, and J. W. Mayer, J. Appl. Phys. **49**, 5199 (1978).
[16] E. A. Stern and S. M. Heald, in *Handbook of Synchrotron Radiation*, edited by D. E. Eastman, Y. Farge, and E. E. Koch (North-Holland, Amsterdam, 1980), Vol. I, Chap. 10; E. A. Stern, B. A. Bunker, and S. M. Heald, Phys. Rev. B **21**, 5521 (1980).
[17] P. A. Lee, P. H. Citrin, P. Eisenberger, and B. M. Kincaid, Rev. Mod. Phys. **53**, 769 (1981).
[18] G. Faraci, A. R. Pennisi, and F. Zontone, Eur. Phys. J. B **51**, 209 (2006); G. Faraci, A. R. Pennisi, F. Zontone, B. Li, and I. Petrov, Phys. Rev. B **74**, 235436 (2006).
[19] J. Mustre de Leon, J. J. Rehr, S. I. Zabinsky, and R. C. Albers, Phys. Rev. B **44**, 4146 (1991); J. J. Rehr, R. C. Albers, and S. I. Zabinsky, Phys. Rev. Lett. **69**, 3397 (1992); M. Newville, J. Synchrotron Radiat. **8**, 322 (2001).
[20] J. J. Rehr, S. I. Zabinsky, A. Ankudinov, and R. C. Albers, Physica B **208/209**, 23 (1995); E. A. Stern, M. Newville, B. Ravel, and Y. Yacoby, *ibid.* **208/209**, 117 (1995).
[21] E. A. Stern, R. W. Siegel, M. Newville, P. G. Sanders, and D. Haskel, Phys. Rev. Lett. **75**, 3874 (1995).
[22] G. Faraci, A. R. Pennisi, A. Balerna, H. Pattyn, G. E. J. Koops, and G. Zhang, Phys. Rev. Lett. **86**, 3566 (2001).
[23] G. Faraci, A. R. Pennisi, R. A. Puglisi, A. Balerna, and I. Pollini, Phys. Rev. B **65**, 024101 (2002).
[24] Matthew Newville, J. Synchrotron Radiat. **8**, 96 (2001); L. F. Smale, C. T. Chantler, M. D. de Jonge, Z. Barnea, and C. Q. Tran, Radiat. Phys. Chem. **75**, 1559 (2006).
[25] A. Filipponi, J. Phys.: Condens. Matter **13**, R23 (2001) and references therein.
[26] P. Fornasini, F. Monti, and A. Sanson, J. Synchrotron Radiat. **8**, 1214 (2001).